Conformational transitions during FtsK translocase activation of individual XerCD–*dif* recombination complexes

Pawel Zawadzki[a], Peter F. J. May[b], Rachel A. Baker[a], Justin N. M. Pinkney[b], Achillefs N. Kapanidis[b,1], David J. Sherratt[a,1], and Lidia K. Arciszewska[a,1]

[a]Department of Biochemistry, University of Oxford, Oxford OX1 3QU, United Kingdom; and [b]Biological Physics Research Group, Department of Physics, University of Oxford, Oxford OX1 3PU, United Kingdom

Edited by Stephen J. Benkovic, The Pennsylvania State University, University Park, PA, and approved September 10, 2013 (received for review June 10, 2013)

Three single-molecule techniques have been used simultaneously and in tandem to track the formation in vitro of single XerCD–*dif* recombination complexes. We observed the arrival of the FtsK translocase at individual preformed synaptic complexes and demonstrated the conformational change that occurs during their activation. We then followed the reaction intermediate transitions as Holliday junctions formed through catalysis by XerD, isomerized, and were converted by XerC to reaction products, which then dissociated. These observations, along with the calculated intermediate lifetimes, inform the reaction mechanism, which plays a key role in chromosome unlinking in most bacteria with circular chromosomes.

tethered fluorophore motion | site-specific DNA recombination | protein–DNA interaction | chromosome segregation | single-molecule FRET

Multiprotein molecular machines mediate most biochemical processes, whose mechanistic understanding requires the combined use of structural and biochemical analyses of wild-type and mutant complexes. Ensemble biochemical and structural analyses lose spatiotemporal resolution through population averaging, thereby limiting mechanistic insight. In contrast, single-molecule techniques provide real-time observation of the dynamics of individual complexes and allow detection of intermediates undetectable with other methods. However, a limitation of many single-molecule techniques is that they only address a single observable and may need considerable information about a system mechanism for the observable to be mechanistically interpreted. Site-specific recombination reactions are ideally suited to single-molecule analysis because they involve discrete complexes that undergo predictably orchestrated catalytic steps. A range of important DNA rearrangements in prokaryotes and simple eukaryotes are mediated by site-specific recombination, which is also widely exploited as a tool in genome engineering (1–3). Tyrosine family recombinases facilitate the propagation of plasmids and viruses, and have key roles in plasmid and chromosome stability and in the horizontal transfer of pathogenicity and antibiotic resistance determinants. The widely distributed XerCD tyrosine recombination system and its orthologs act in chromosome and plasmid segregation and stability in most bacteria, by converting chromosome and plasmid dimers to monomers and by acting in the decatenation of linked chromosomes (1, 2, 4, 5).

Extensive ensemble biochemical and structural studies have shown that tyrosine recombinases share a common reaction mechanism in which a tyrosine nucleophile catalyzes recombination in two steps, with Holliday junctions (HJs) as essential reaction intermediates. Reciprocal activation–inactivation of recombinase pairs occurs during HJ isomerization as the reaction proceeds (2, 6, 7). The paradigm for this mechanism comes from biochemical and structural studies of Cre–*loxP* recombination (2, 6, 8–10) (Fig. 1*A*).

XerCD recombination systems typically use two different yet related recombinases, XerC and XerD, each of which mediates exchange of a specific pair of strands: "top" and "bottom" strands, respectively (Fig. 1*B*). In some bacteria, XerCD has been replaced by a single polypeptide, XerS (11). XerCD can act on a variety of recombination sites naturally present in plasmids and chromosomes with different requirements and outcomes. Recombination at *dif*, a site located in the replication terminus region of the chromosome, requires activation by the DNA translocase, FtsK.

Although the XerCD–*dif*–FtsK reaction has been studied extensively using ensemble biochemical experiments, the lack of structures of the recombinases bound to DNA has limited progress in understanding the detailed reaction mechanism. In the absence of FtsK, XerC can catalyze HJ formation and resolution in vivo and in vitro with no detectable formation of product by XerD (12, 13). In contrast, in the presence of FtsK, recombination is initiated by XerD, giving HJs that can isomerize to form a substrate that allows completion of recombination by XerC (12, 14) (Fig. 1*C*). Until now, it has been unclear how FtsK action gives rise to synaptic structures that can be acted on by XerD, although it has been proposed previously that FtsK actively remodels a synaptic complex that was initially poised to undergo catalysis by XerC (14). Such a remodeling would require dissociation of XerCD–*dif* complexes and reassembly in a different conformation, if the reaction follows the Cre–*loxP* paradigm.

Here, we report a detailed analysis of XerCD–*dif*–FtsK recombination within individual synaptic complexes in real time. By using three simultaneous and independent observables, Förster resonance energy transfer (FRET), tethered fluorophore motion

Significance

Insight into the mechanisms that underlie the process of faithful chromosome segregation is of importance for understanding the place of humans in the living world. Bacteria are the most abundant free-living organisms and have important roles in human health and disease. Nevertheless, molecular understanding of bacterial chromosome segregation is in its infancy. In this paper, the action of one conserved molecular machine that acts to coordinate the late steps of chromosome segregation with cell division is analyzed molecule by molecule in real time, using three complementary single-molecule techniques simultaneously. By using normal and mutated proteins, the complete reaction pathway is revealed from assembly of the initial nucleoprotein complex, to its activation by a DNA motor, and to the subsequent steps that lead to chromosome unlinking.

Author contributions: D.J.S. and L.K.A. conceived and directed the project; A.N.K., D.J.S., and L.K.A. supervised the project. P.Z., P.F.J.M., and J.N.M.P. undertook research and data interpretation; R.A.B. provided reagents; and P.Z., P.F.J.M., A.N.K., D.J.S., and L.K.A. wrote the paper.

The authors declare no conflict of interest.

This article is a PNAS Direct Submission.

Freely available online through the PNAS open access option.

[1]To whom correspondence may be addressed. E-mail: lidia.arciszewska@bioch.ox.ac.uk, kapanidis@physics.ox.ac.uk, or david.sherratt@bioch.ox.ac.uk.

This article contains supporting information online at www.pnas.org/lookup/suppl/doi:10.1073/pnas.1311065110/-/DCSupplemental.

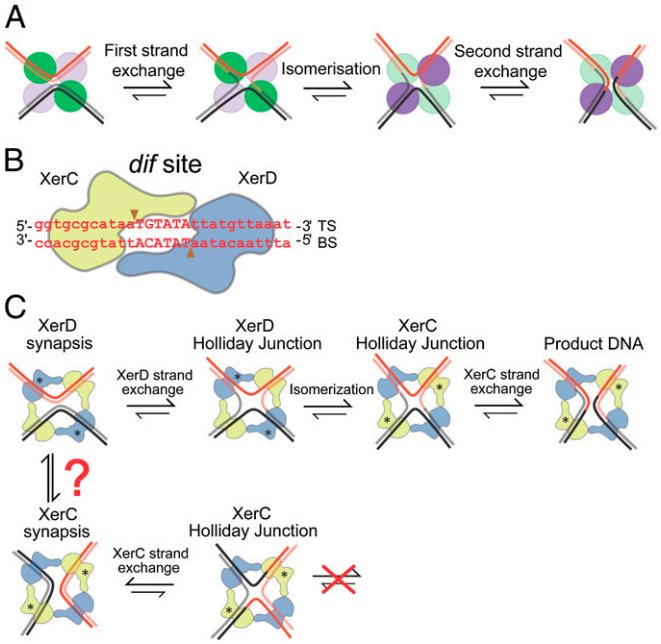

Fig. 1. Tyrosine family site-specific recombination. (*A*) Schematic showing tyrosine recombinase pathway. The green and violet circles indicate recombinase protomers, with the color being highlighted when a given recombinase pair is active. Isomerization of the HJ intermediate plays an essential role in the reciprocal catalytic switches in recombinase activity. (*B*) XerCD–*dif* core site. XerC (yellow) and XerD (blue) bind to their respective DNA *dif* half-sites. TS and BS are the "top" and "bottom" strands, respectively. The scissile phosphates, indicated by the arrowheads, flank the central region, TGTATA. (*C*) XerCD–*dif* recombination at *dif* as envisaged using the Cre–*loxP* paradigm (6) (active monomers are labeled with asterisks). FtsK activated pathway is shown at the *Top*; an XerD-active synapsis (XerD*) leads to a XerD–HJ, which is subsequently isomerized to a XerC–HJ, which is resolved by XerC to recombinant products. In the absence of FtsK, XerCD–*dif* synaptic complexes (XerC*) can form and undergo cycles of XerC-mediated strand exchanges (*Bottom*). XerC and XerD synaptic complexes can only be interconverted by changing the path of the DNA helix in a complex, or by breaking the recombinase–recombinase interactions involved in synapsis and reforming the complementary synaptic complex de novo.

(TFM) and protein-induced fluorescence enhancement (PIFE), we were able to follow the long-range and nanoscale dynamics of the complete recombination reaction. We observed the arrival of the FtsK translocase at an initial synaptic complex, and the conformational change that FtsK induced during recombination activation, forming a transient activated complex in which XerD exchanged a pair of strands to form an HJ intermediate. Isomerization of the HJ formed a substrate for catalysis by XerC, thereby leading to complete recombinant product, which then dissociated into its duplex components.

Results

XerCD–*dif* Synaptic Complexes. To characterize the assembly and architecture of synaptic complexes, we used TFM in combination with single-molecule FRET by implementing alternating laser excitation on a total internal reflection microscope (15, 16). This allowed simultaneous monitoring of large-scale conformational changes in DNA and nanoscale changes within the nucleoprotein complexes. The substrates were 4-kbp–long DNA molecules, which contained two repeated *dif* sites separated by 1 kbp; they were tethered to a PEG-passivated glass coverslip using a biotin–NeutrAvidin interaction. A 2.8-kbp DNA extension containing an FtsK loading site beyond the distal *dif* site facilitated efficient loading of FtsK onto DNA. The substrates were labeled adjacent to the *dif* sites with a FRET donor (Cy3B) and acceptor (Cy5) (Figs. 2*A*, 3*A*, and 4*A*, and Fig. S1). In all substrates, the acceptor fluorophore was separated from the surface by >1 kbp of linear B-DNA (with a contour length of ∼300 nm). The persistence length of DNA is around 50 nm, so the surface distal fluorophore is allowed considerable diffusional freedom around the tether point. Because this motion occurs on a millisecond timescale, the in-plane motion of the fluorophore about the surface is evidenced by a blurring of the associated point spread function (PSF) in the 100-ms camera exposures (15). XerCD-mediated formation of a synaptic complex between two *dif* sites was expected to reduce this diffusional freedom of the distal fluorophore, which would reduce the PSF width. This reduction in PSF width is the main TFM observable.

Substrate I design was informed by the Cre–*loxP* crystal structure (2HOI) (17), and was similar to that used by Pinkney et al. (15) (Fig. 2*A* and Fig. S1*A*). It was expected to give recombination intermediates having interfluorophore distances of less than 90 Å during early stages of the recombination reaction, thereby giving rise to apparent FRET efficiencies of $E^* > 0.2$ (Table S1). When this substrate was reacted with XerCD in the absence of FtsK, we observed reversible cycles of transient narrowing of PSF, consistent with the assembly and disassembly of synaptic complexes that did not undergo recombination, as expected, because FtsK is required for initiation of catalysis by XerD (Fig. 2*B*, *Bottom*). The narrowing of the PSF was accompanied by the appearance of FRET, with $E^* \approx 0.55$ (Fig. 2*B*, *Middle*), corresponding to an interfluorophore distance of ≈59 Å (Tables S2 and S3 and *Materials and Methods*). The mean lifetime $\tau = 8.6$ s of these initial synaptic complexes was obtained from a single exponential fit to the dwell time distribution (Fig. 2*B*, *Inset*). A minority (<9%) of narrowing events were not accompanied by any apparent FRET, which we attribute to nonspecific sticking of protein–DNA complexes to the surface.

FtsK Activates Recombination on Initial Synaptic Complexes. To test whether the above initial synaptic complexes were substrates for the activation of recombination by FtsK, we repeated the same experiments using substrate I in the presence of FtsK and ATP. We observed two predominant complexes: ones similar to those in Fig. 2*B*, exhibiting simultaneous disappearance of FRET, and PSF broadening, indicative of synaptic complex formation and dissociation (Fig. S2*A*); and complexes indicative of successful recombination (Fig. 2*C*), in which FRET was lost but a narrow PSF remained. The lifetime of these latter complexes was significantly shorter (τ = 4.0 s; Fig. 2*C*, *Inset*) than that of initial complexes that formed in the absence of FtsK (τ = 8.6 s), indicating efficient activation of synaptic complexes by FtsK.

To gain further insight into the recombination mechanism, we used substrate II (Fig. 3*A* and Fig. S1*B*), which using the Cre–*loxP* crystal structure (2HOI) as a template was labeled at sites that should allow detection of intermediates preceding HJ isomerization (Table S1). Additionally, upon completion of recombination and dissociation of the product, both fluorophores should disappear from view simultaneously (Fig. 3*A*). Due to the different labeling position, the initial complexes in the absence of FtsK had an $E^* \approx 0.72$ (Fig. 3*B*), higher than in substrate I; nevertheless, the lifetime of these complexes without FtsK (τ = 8.1 s; Fig. S3*A*) was comparable to those observed with substrate I (τ = 8.6 s).

In the presence of FtsK and ATP, we observed discrete transitions from the initial synaptic complex with $E^* \approx 0.72$ and a narrow PSF (Fig. 3*C*, yellow highlight) to a short-lived intermediate that retained the narrow PSF, but had $E^* \approx 0.37$ (Fig. 3*C*, green highlight); followed by a low FRET state with $E^* \approx 0.18$ (Fig. 3*C*, cyan highlight); followed by simultaneous loss of both fluorophores, indicative of the completion of recombination and dissociation of the reaction products (Fig. 3*C*, black arrow). We interpret these three FRET states as follows: $E^* \approx 0.72$ defines the initial synaptic complexes; $E^* \approx 0.37$ describes synaptic complexes in which XerD is active (XerD*) and/or the XerD–HJ resulting from strand exchange by XerD on XerD*; finally $E^* \approx 0.18$ complexes consist of HJ intermediates following isomerization,

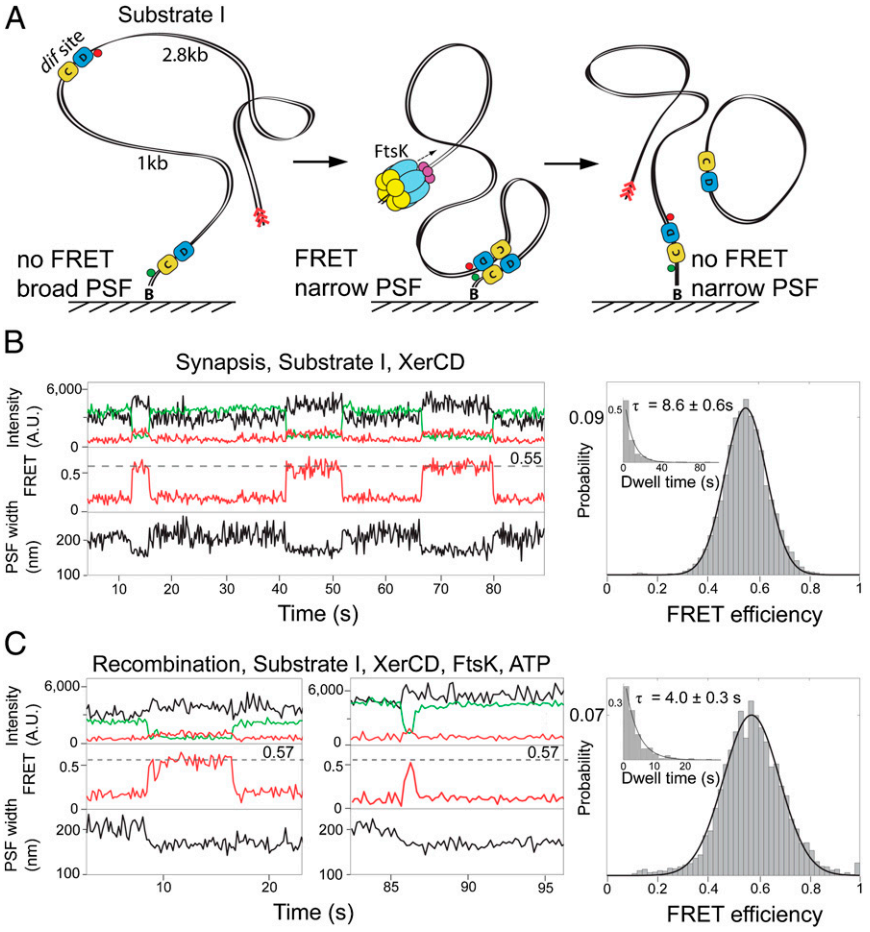

Fig. 2. XerCD–*dif* synapsis and recombination. (*A*) Schematic of the recombination reaction with substrate I. Substrate I has the fluorophores attached to DNA adjacent to each *dif* site; the positions of the acceptor and the donor fluorophores are indicated with red and green circles, respectively (Fig. S1*A*). Progression through the recombination was monitored using two observables: PSF width of the acceptor and FRET. Recombination between two *dif* sites leads to a formation of product DNA molecules, one of them remains attached to the slide and has fluorophores flanking *dif* on both sides. The preferential binding site for FtsK, KOPS (FtsK orientation polarizing sequence), is indicated with red arrowheads. (*B*) Nonproductive synaptic complexes (*Top*). Representative time trace of the intensities of donor (green), and acceptor (red) under donor excitation; and acceptor under acceptor excitation (black). FRET efficiency (*Middle*) and PSF width (*Bottom*) are shown. The nonproductive events are defined by the ultimate broadening of the PSF coincident with the disappearance of the FRET signal. All data were acquired at a frame rate of 10 Hz, unless otherwise stated. Histogram (*Right*) of FRET efficiency (*E**) and dwell time (*Inset*) of XerCD–*dif* synaptic complexes (n = 380). Dwell times were fit to single exponentials. (*C*) Recombining complexes. The complexes were identified by the persistence of a low PSF after the disappearance of FRET. Two representative time traces are shown, along with histograms of FRET efficiency and dwell times of recombining complexes (n = 249; *Right*).

where XerC is active (XerC–HJs), and the product DNA complexes (XerC–Ps), resulting from strand exchange by XerC on XerC–HJs. Note that the XerC–HJ and the XerC–P states (Fig. 3*C*) are sufficiently close to the background $E^* \approx 0.17$ (*Materials and Methods*) that they are essentially indistinguishable.

To validate this interpretation, we analyzed reactions using catalytically inactive mutants of XerC and XerD [XerC^{KQ} (K172Q) and XerD^{KQ} (K172Q); Fig. 3 *D* and *E*] in the presence of their wild-type protein partners using substrate II. The reactions containing XerC^{KQ} and XerD gave synaptic complexes with $E^* \approx 0.72$, indistinguishable from the wild-type XerCD complexes (Fig. S3*B*). In the presence of FtsK and ATP, these complexes yielded two rapidly interconverting FRET states (Fig. 3*D*). Analysis of the interconverting FRET states with hidden Markov modeling (HMM) (*Materials and Methods*) (18) revealed that the interconversion occurred between $E^* \approx 0.37$ and $E^* \approx 0.22$ (Fig. S3*D*). We interpret these interconversions as isomerization between XerD–HJ and XerC–HJ states, because XerC^{KQ} cannot catalyze the final HJ resolution to product and accumulates HJs in bulk assays (13). Furthermore, resolution of the interconverting FRET states always progressed through a high FRET state, indicative of the initial synaptic complex ($E^* \approx 0.72$; Fig. 3*D*, purple). This shows that the initial complex ($E^* \approx 0.72$) is an obligatory intermediate in XerCD–*dif* recombination and that XerD–HJs can be resolved by XerD to initial synaptic complexes, at least in the presence of XerC^{KQ}.

Reaction of XerC with XerD^{KQ} in the absence of FtsK and ATP produced synaptic complexes with $E^* \approx 0.72$ (Fig. S3*C*), similar to the initial synaptic complexes formed by wild-type XerCD. We expected that these would be susceptible to FtsK-mediated remodeling to XerD*, but that they would not be able to progress to XerD–HJ. Indeed, an FtsK-dependent interconversion between states with $E^* \approx 0.72$ and $E^* \approx 0.44$ was observed (Fig. 3*E* and Fig. S3*E*). These results established that remodeling of the initial complex precedes catalysis by XerD. We note that the $E^* \approx 0.44$, assigned here for XerD*, is significantly different from the $E^* \approx 0.37$ for XerD–HJ determined in complexes with XerC^{KQ}D (Fig. 3*D*) and again different from XerD*/XerD–HJ observed in recombining complexes (Fig. 3*C*, $E^* \approx 0.37$). We propose that the $E^* \approx 0.37$ state, observed in recombining complexes, represents mostly XerD–HJ with XerD* being transient. Because XerD* and XerD–HJ differ in E^*, we suggest that they differ in overall architecture. We converted $E^* \approx 0.37$ and $E^* \approx 0.44$ into distances (*Materials and Methods* and Table S2), and found that the interfluorophore distance differed by 5 ± 15 Å, with the majority of the uncertainty in all FRET-derived distances in our work attributed to uncertainty in the orientation factor of the fluorophores, κ^2.

PIFE Monitors the Arrival of FtsK at the Initial Synaptic Complex. To study the final steps of recombination we designed a third substrate within which the fluorophores flanked the distal *dif* site and again, using the Cre–*loxP* structure as a template, were positioned to show FRET after HJ isomerization, with dissociation of product DNA leading to a loss of FRET and loss of the donor fluorophore (Fig. 4*A*, Fig. S1*C*, and Table S1). In the absence of FtsK and ATP, we detected the formation of synaptic complexes, inferred from simultaneous narrowing of both donor and acceptor PSFs (Fig. S4*A*). In the presence of FtsK and ATP, equivalent synaptic complexes were observed, as well as complexes indicating productive recombination. The latter showed narrowing of PSF subsequently followed by a transition to an $E^* \approx 0.56$ state (Fig. 4*B*); followed by a transition to an $E^* \approx 0.40$ state; and then recombinant product dissociation monitored by the loss of donor fluorescence. Transition back to the $E^* \approx 0.56$ state from the $E^* \approx$

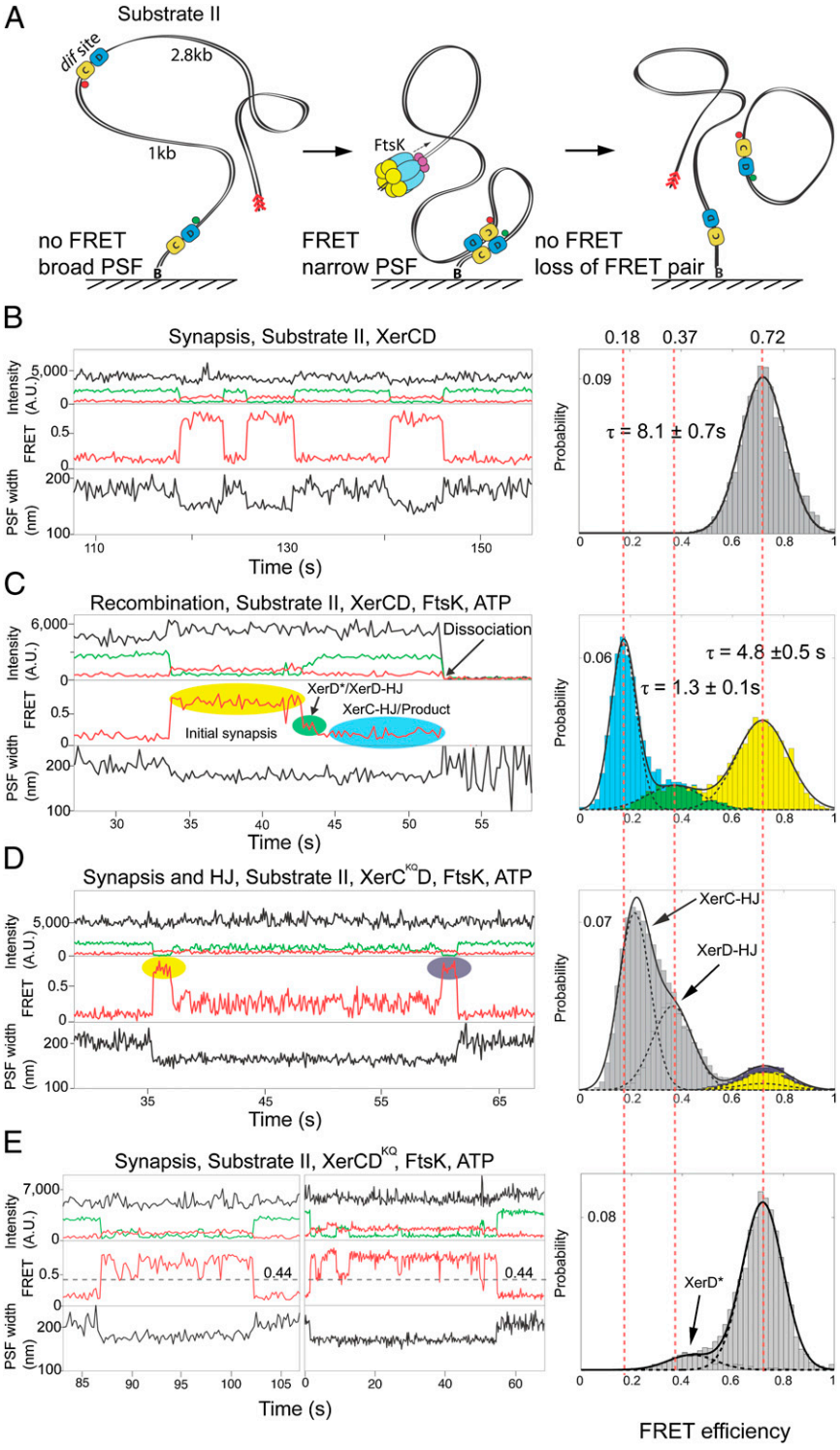

Fig. 3. XerCD–*dif*–FtsK recombination intermediates. (*A*) A cartoon of the recombination reaction within substrate II (Fig. S1*B*). Recombination of this substrate generates a circular DNA product, carrying both fluorophores; its dissociation was assayed by the simultaneous disappearance of both red and green fluorescence emission. (*B*) Initial synaptic complexes in the absence of FtsK. A representative time and a histogram of FRET efficiency are shown. The mean lifetime of the synapses, τ, is indicated ($n = 382$; Fig. S3*A*). (*C*) Productive recombination events in the presence of FtsK–ATP. Intermediates of recombination were distinguished by their different apparent FRET efficiencies. The following intermediates could be identified: initial synaptic complex (highlighted yellow), XerD–active synaptic complexes, XerD*, and/or XerD HJ (green), and XerC HJ/XerC product (XerC–P) (cyan). Dissociation of the complex upon completion of recombination is indicated in the time trace with an arrow. Color-coded histograms of FRET efficiencies for each step and the mean lifetimes, τ, are shown on the *Right* ($n = 134$; Fig. S3*A*). We note good agreement between the lifetime of the high FRET state between substrates I and II, shown in this figure and in Fig. 2*C*. The dwell times indicated are for individual transitions, not the entire reaction. To complete the kinetics of the pathway, it is necessary to combine rates from all three substrates. (*D*) Complexes in the presence of XerC^{KQ}D and FtsK. Data were taken with a frame rate of 20 Hz. The complexes were transiently trapped at the HJ intermediate stage, and exhibited a rapid interconversion between $E^* \approx 0.22$ and ≈ 0.37, suggesting rapid isomerization between XerC–HJ and XerD–HJ. These complexes assembled in the initial conformation (highlighted yellow) and adopted the same conformation before dissociation (purple). Histograms of FRET efficiencies are shown on the *Right* ($n = 84$). (*E*) Complexes in the presence of XerCD^{KQ} and FtsK. The representative time traces display multiple reversible reductions in FRET signal to $E^* \approx 0.44$, suggesting the transient formation of XerD*. A histogram of FRET efficiencies is shown on the *Right* ($n = 66$).

0.40 state were also occasionally observed (Fig. S4*B*). Because XerC–HJs precede XerC–Ps and the $E^* \approx 0.56$ state preceded the lower $E^* \approx 0.40$ state, we conclude that $E^* \approx 0.56$ corresponds to XerC–HJ and $E^* \approx 0.40$ corresponds to XerC–P. This is supported by experiments using XerC^{KQ} and wild-type XerD with this substrate (Fig. S5). We infer from the above reversible transitions that XerC–P can be converted to XerC–HJ by XerC-mediated catalysis. Because XerC–HJ and XerC–P differ in E^*, we infer that they differ in architecture. By converting E^* to distance (*Materials and Methods* and Table S2), we found that the interfluorophore distance changed by 8 ± 13 Å between XerC–HJ and XerC–P. Taken together with the difference in E^* between XerD* and XerD–HJ discussed in the previous section, these changes show that structural rearrangements occur after strand exchange by both XerC and XerD.

The proximity of a protein to an organic fluorophore can enhance or quench its fluorescence. Tryptophan residues can participate in a photoinduced electron transfer process, quenching fluorescence (19). However, for dyes that can undergo a *cis–trans* isomerization, the proximity of a protein can reduce the rate of isomerization to the photoinactive *cis* state, increasing the

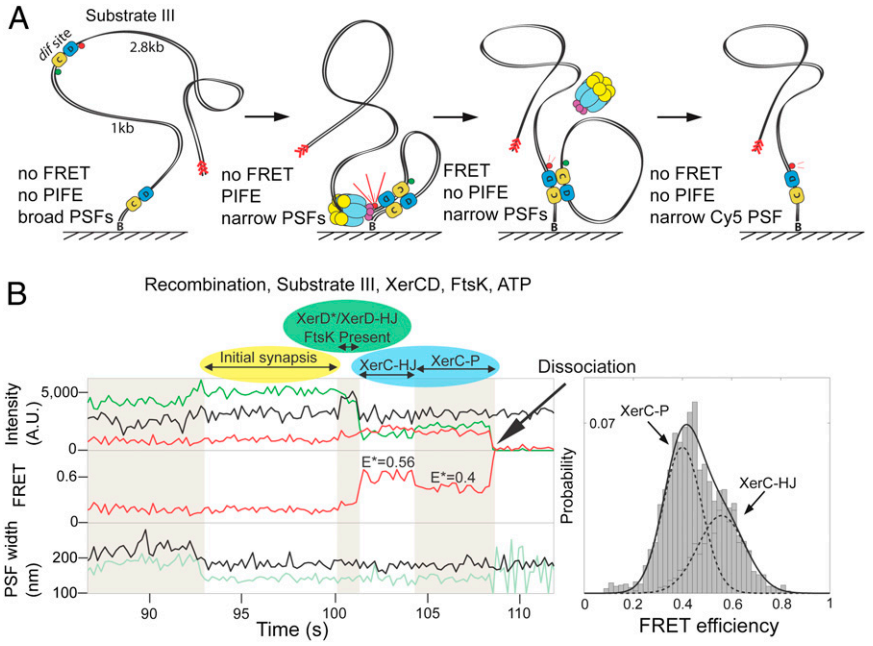

Fig. 4. Activation by FtsK. (*A*) Schematic of recombination within substrate III (Fig. S1*C*). The fluorophores are flanking a distal *dif* site. On completion of recombination and complex dissociation, the donor fluorophore is lost. Multiple steps during recombination can be distinguished using three observables: PSF, FRET, and PIFE. (*B*) Representative time trace showing the progression of the recombination with this substrate. The color coding of various states is the same as in Fig. 2*C*: initial complex, yellow; XerD*/XerD–HJ, green; XerC–HJ/XerC–P, cyan. The increase in acceptor intensity (*Top*, black line, at ≈100 s), as a consequence of PIFE, is indicative of the presence of FtsK at XerCD–*dif* and is preceded by simultaneous narrowing of PSFs for both donor (pale green) and acceptor (black), indicative of initial synapse formation. A histogram showing FRET efficiency was fit with two Gaussians (n = 111), having separated the two states using HMM (*Materials and Methods*). The dwell times for XerC–HJs and XerC–Ps are shown in Fig. S4*B*.

quantum yield of the fluorophore. This enhancement is termed PIFE (20). Substrate III allowed us to monitor the arrival of FtsK at synaptic complexes using PIFE of the acceptor fluorophore (Fig. 4*A*). We observed that in 77% of the recombination events monitored, the transition between the initial synaptic complex and the XerC–HJ was accompanied by PIFE of the acceptor fluorophore (Fig. 4*B*, *Top*, highlighted green, and Fig. S4*C*). This confirms that FtsK activates preformed initial complexes. Disappearance of PIFE was concomitant with the emergence of the FRET signal hallmarking isomerization of the HJ (Fig. 4*B*, *Top* and *Middle*, and Fig. S4*D*). The loss of PIFE upon HJ isomerization to form XerC–HJ, could result either from FtsK moving away from the vicinity of the recombining complex (for example, by dissociation, or by reversing translocation), or from a change in conformation of the FtsK-recombining complex. Reversals of translocation have been reported previously (21–23). Observation of PIFE with substrate I suggested the same sequence of events (Fig. S4*E*).

Discussion

The use of three independent observables, FRET, PSF width, and PIFE, has allowed us to monitor long-range substrate DNA movements that occur during the formation of single XerCD–*dif* synaptic complexes, along with the nanoscale conformational transitions that occur within the nucleoprotein complexes as the recombination reaction proceeds. This analysis has provided direct information on the recombination pathway. Taken together, the results lead us to propose the reaction pathway shown in Fig. 5. Spontaneously formed initial synaptic complexes can be acted on directly by FtsK, leading to a conformational change that results in the formation of a transient synaptic complex (XerD*) in which XerD is poised to undergo catalysis, thereby generating the XerD–HJ intermediate. Isomerization of this HJ intermediate leads to a XerC–HJ, which can then be reacted on by XerC, giving a recombinant product synaptic complex that dissociates quickly. Following the initial activation step, the proposed recombination pathway is broadly similar to the established Cre–*loxP* paradigm for tyrosine recombinases (6, 8–10). Nevertheless, we note that in the Cre–*loxP* structures, the architecture of a synaptic complex is almost identical to the HJ intermediate that is generated from it (8–10). In contrast, our FRET measurements indicate discrete conformational changes in architecture as the HJ forms and resolves (Fig. 5), perhaps committing the reaction to a more directional outcome.

Our observation that PIFE resulting from FtsK arrival at a synaptic complex is transient and disappears as XerC–HJs form, indicates that a functional change occurs in the complex at this point of the reaction. This could be a local change in FtsK position or conformation, or one that leads to FtsK dissociation. Nevertheless, we note that in reactions of $XerD^{KQ}$ and XerC on substrate II, FtsK is able to make repeated cycles of apparent activation, suggesting that in situations where recombination is nonproductive, FtsK remains in the proximity of the synaptic complex. Similarly, our observation that XerD can catalyze the resolution of HJs in the presence of $XerC^{KQ}$ and FtsK lends support to the view that FtsK can remain in the vicinity of the synaptic

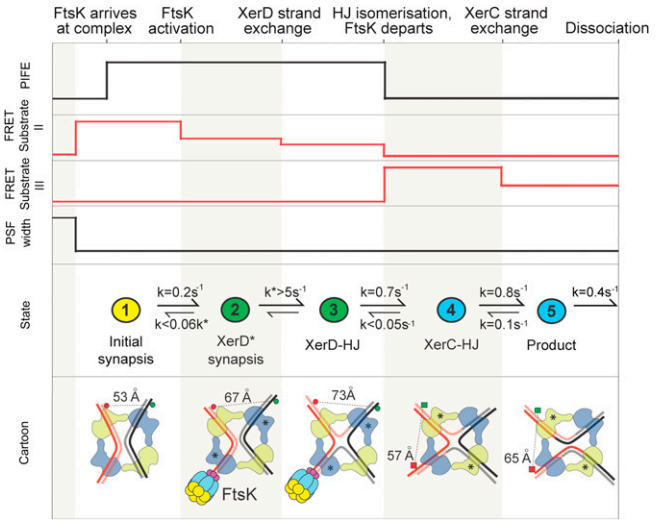

Fig. 5. FtsK-activated XerCD–*dif* recombination. (*Top* and *Middle*) Summary of the changes in PSF, FRET, and PIFE states of the reactions on substrates II and III, with rate constants deduced from intermediate lifetimes (*Materials and Methods*). The colors in the *Middle* correspond to those used in Figs. 2–4. (*Bottom*) The proposed architectures of the initial, intermediate, and final complexes based on the interfluorophore distances derived from analyses with substrate II (fluorophore pairs indicated with circles) and substrate III (fluorophore pairs indicated with squares). Limits on reverse rates have been estimated given the rarity of backward transitions (2%).

complex as recombination proceeds, consistent with the multiple rounds of recombination that are expected to occur during decatenation (5).

Our experiments have specifically addressed the pathway of recombination activated by FtsK, in which XerD initiates catalysis. The requirement for the FtsK activation step distinguishes this pathway from that undertaken in Cre–*loxP* recombination. The observation that FtsK appears to act on preformed synaptic complexes is consistent with an earlier report showing that a single translocating FtsK hexamer is sufficient to activate recombination on a XerCD–*dif* synaptic complex (24). The observation argues against models in which activation occurs on duplexes before synapsis (for example, by promoting XerD* synaptic complex formation), or in which FtsK actively remodels a complex that was initially poised to undertake catalysis by XerC (14). Because FtsK acts on preexisting synaptic complexes that undergo directly a conformational change to form XerD* complexes, the substrate for catalysis by XerD, suggests that XerC* synaptic complexes form independently. The presence and action of XerC* complexes has been inferred from ensemble studies in vivo and in vitro by the demonstration of XerC-catalyzed HJ formation and resolution in the absence of FtsK (12, 14, 25). Our assays have not revealed insight into XerC* formation, because *dif*–XerCD synaptic complexes of narrow PSF and the expected FRET values (Fig. 3*B* and Fig. S4*A*) were not detected, suggesting they are too infrequent to be investigated with our assay. Nevertheless, we inferred XerC-catalyzed formation of XerC–HJs from XerC–P complexes ($k = 0.1\ s^{-1}$) in reactions initiated by XerD-mediated catalysis (Fig. 5); note that XerC* complexes are expected to be identical to XerC–Ps.

Studies of the "XerC-first" pathway in which XerC* complexes generate XerC–HJs have not previously yielded evidence that FtsK can promote the isomerization of XerC–HJs to XerD–HJs, which then undergo catalysis by XerD (25). Nevertheless, the observation that HJs made by XerD, in the presence of $XerC^{KQ}$ and FtsK, can be converted back to substrate by XerD-mediated catalysis, shows that this pathway is possible, although it may not be favorable with wild-type XerCD. In our view, the XerC-first pathway is unlikely to be significant in vivo.

Given the intracellular concentrations of XerCD and their avid binding to *dif* sites, we believe it likely that *dif* sites in vivo are largely recombinase bound. Therefore, sister *dif* sites may synapse with high efficiency immediately after their duplication at the termination of replication. Those in a conformation suitable for activation by FtsK will still synapse, whereas those in the XerC* conformation will be stabilized by cycles of XerC-mediated HJ formation and resolution. We would not expect XerC* and XerD* complexes to be interconvertible without dissociation into their duplex components (Fig. 1). Together, these processes may help sister *dif* sites remain in proximity.

Once FtsK loads onto a chromosome, its translocation toward XerCD-bound *dif* will lead to the formation of activated XerD* complexes that undergo a complete recombination reaction. The temporal and spatial organization of FtsK activity in the region of *dif* will ensure that complete recombination reactions on the initial complexes, revealed in this work, will be limited to the septal region of the cell and to late stages of the cell cycle, thereby safeguarding against inappropriate recombination. Future work will address further mechanistic details of the FtsK activation mechanism and how this relates to the simplification of topology during FtsK-activated XerCD–*dif* recombination on circular DNA substrates.

Materials and Methods

Standard techniques for DNA labeling and protein purification were used and are described in detail in *SI Text*. Single-molecule experiments are described in *SI Text*. Details and procedures for data analysis and accurate FRET and distance calculation and simulations are also presented in *SI Text*.

ACKNOWLEDGMENTS. Work in the D.J.S. laboratory was supported by Wellcome Trust Program Grant WT083469MA. J.N.M.P. was supported by the UK Engineering and Physical Sciences Research Council, and P.F.J.M. was supported by MathWorks. A.N.K. was supported by European Commission Seventh Framework Programme Grant FP7/2007-2013 HEALTH-F4-2008-201418, Biotechnology and Biological Research Council Grant BB/H01795X/1, and European Research Council Starter Grant 261227.

1. Grindley NDF, Whiteson KL, Rice PA (2006) Mechanisms of site-specific recombination. *Annu Rev Biochem* 75:567–605.
2. Hallet B, Sherratt DJ (1997) Transposition and site-specific recombination: Adapting DNA cut-and-paste mechanisms to a variety of genetic rearrangements. *FEMS Microbiol Rev* 21(2):157–178.
3. Akopian A, Marshall Stark W (2005) Site-specific DNA recombinases as instruments for genomic surgery. *Adv Genet* 55:1–23.
4. Sherratt DJ, et al. (1995) Site-specific recombination and circular chromosome segregation. *Philos Trans R Soc Lond B Biol Sci* 347(1319):37–42.
5. Grainge I, et al. (2007) Unlinking chromosome catenanes in vivo by site-specific recombination. *EMBO J* 26(19):4228–4238.
6. Van Duyne GD (2001) A structural view of Cre-loxP site-specific recombination. *Annu Rev Biophys Biomol Struct* 30:87–104.
7. Nunes-Düby SE, Kwon HJ, Tirumalai RS, Ellenberger T, Landy A (1998) Similarities and differences among 105 members of the Int family of site-specific recombinases. *Nucleic Acids Res* 26(2):391–406.
8. Guo F, Gopaul DN, van Duyne GD (1997) Structure of Cre recombinase complexed with DNA in a site-specific recombination synapse. *Nature* 389(6646):40–46.
9. Gopaul DN, Guo F, Van Duyne GD (1998) Structure of the Holliday junction intermediate in Cre-loxP site-specific recombination. *EMBO J* 17(14):4175–4187.
10. Guo F, Gopaul DN, Van Duyne GD (1999) Asymmetric DNA bending in the Cre-loxP site-specific recombination synapse. *Proc Natl Acad Sci USA* 96(13):7143–7148.
11. Nolivos S, Pages C, Rousseau P, Le Bourgeois P, Cornet F (2010) Are two better than one? Analysis of an FtsK/Xer recombination system that uses a single recombinase. *Nucleic Acids Res* 38(19):6477–6489.
12. Barre F-X, et al. (2000) FtsK functions in the processing of a Holliday junction intermediate during bacterial chromosome segregation. *Genes Dev* 14(23):2976–2988.
13. Grainge I, Lesterlin C, Sherratt DJ (2011) Activation of XerCD-dif recombination by the FtsK DNA translocase. *Nucleic Acids Res* 39(12):5140–5148.
14. Aussel L, et al. (2002) FtsK Is a DNA motor protein that activates chromosome dimer resolution by switching the catalytic state of the XerC and XerD recombinases. *Cell* 108(2):195–205.
15. Pinkney JNM, et al. (2012) Capturing reaction paths and intermediates in Cre-loxP recombination using single-molecule fluorescence. *Proc Natl Acad Sci USA* 109(51):20871–20876.
16. Kapanidis AN, et al. (2004) Fluorescence-aided molecule sorting: Analysis of structure and interactions by alternating-laser excitation of single molecules. *Proc Natl Acad Sci USA* 101(24):8936–8941.
17. Ghosh K, Guo F, Van Duyne GD (2007) Synapsis of loxP sites by Cre recombinase. *J Biol Chem* 282(33):24004–24016.
18. Uphoff S, Gryte K, Evans G, Kapanidis AN (2011) Improved temporal resolution and linked hidden Markov modeling for switchable single-molecule FRET. *ChemPhysChem* 12(3):571–579.
19. Doose S, Neuweiler H, Sauer M (2005) A close look at fluorescence quenching of organic dyes by tryptophan. *ChemPhysChem* 6(11):2277–2285.
20. Hwang H, Kim H, Myong S (2011) Protein induced fluorescence enhancement as a single molecule assay with short distance sensitivity. *Proc Natl Acad Sci USA* 108(18):7414–7418.
21. Pease PJ, et al. (2005) Sequence-directed DNA translocation by purified FtsK. *Science* 307(5709):586–590.
22. Saleh OA, Pérals C, Barre F-X, Allemand J-F (2004) Fast, DNA-sequence independent translocation by FtsK in a single-molecule experiment. *EMBO J* 23(12):2430–2439.
23. Lee JY, Finkelstein IJ, Crozat E, Sherratt DJ, Greene EC (2012) Single-molecule imaging of DNA curtains reveals mechanisms of KOPS sequence targeting by the DNA translocase FtsK. *Proc Natl Acad Sci USA* 109(17):6531–6536.
24. Massey TH, Aussel L, Barre FX, Sherratt DJ (2004) Asymmetric activation of Xer site-specific recombination by FtsK. *EMBO Rep* 5(4):399–404.
25. Arciszewska LK, Baker RA, Hallet B, Sherratt DJ (2000) Coordinated control of XerC and XerD catalytic activities during Holliday junction resolution. *J Mol Biol* 299(2):391–403.

Supporting Information

Zawadzki et al. 10.1073/pnas.1311065110

SI Text

DNA and Protein Preparation. The 1-kb DNA substrates were prepared via a PCR using two fluorescently labeled oligonucleotides as primers and a plasmid template containing directly repeated *dif* sites separated by a 1-kb KmR gene cassette (pRB10). Phusion High-Fidelity DNA polymerase (NEB) was used.

The oligonucleotides used were as follows: substrate I, forward, 5′-GTGTCGACACAXGATTTAACATAAT-3′, and reverse, 5′-CTCTAGACCATGGAXCATGTGGTGCGCATA-3′; substrate II, forward, 5′-CATGTGTCGACACATGATTTAACATAATA-TACATTATGCGCACCACATGXAGCTGAGATCTG-3′, and reverse, 5′-AGACCATGGCATGTGGTGCGCATAATGTA-TATTATGTTAAATCXTGTGGATCCAC-3′; substrate III, forward, 5′-TAGCGTCGACCTACAXGATTTAACATAATA-TACATTATGCGCACCAAATGATTCGCAGCTGAGATC-3′, and reverse, 5′-GATCGATCTCAGCTGCGAAXCATTTG-GTGCGCATAATGTATATTATGTTAAATCATGTAGGT-CGACGCTA-3′, where X indicates the position of 5-C6-amino dT. Forward and reverse oligonucleotides were labeled at the X positions with Cy5 and Cy3B, respectively. Oligonucleotides were synthesized and HPLC purified by ATDBio Ltd. Cy5 labeling was performed by ATDBio, and Cy3B labeling was performed as previously described (1). After PCRs, the products were NcoI digested and ligated to a biotin-labeled 200-bp extension (produced using PCR). Subsequently, a long (2.8-kb) DNA tail was ligated to the opposite end (following a SalI digestion) and the 4-kb substrate was gel purified. The tail acts as a loading site for FtsK; recombination was never observed in our assays in substrates without it. Substrate III was prepared with unlabeled oligonucleotides, otherwise identical to those used in substrate I preparation. Subsequently, the distal *dif* site was removed by digestion with BglII and an identical sequence, produced by the annealing of two fluorophore-labeled oligonucleotides, was ligated back.

XerC, XerD, and FtsK trimer were purified according to previously published procedures (2, 3).

Instrumentation. Single-molecule total internal reflection fluorescence (TIRF) experiments were performed on a custom-built objective type TIRF microscope. A green (532-nm Cobolt Samba) and red (635-nm Cube Coherent) laser were combined using a dichroic mirror and coupled into a fiber optic cable. The output of the fiber was focused into the back focal plane of the objective (100°—oil immersion; numerical aperture, 1.4; Olympus) and displaced perpendicular to the optical axis such that laser light was incident at the slide–solution interface at greater than the critical angle, creating an evanescent excitation field. Alternating laser excitation was implemented by directly modulating the lasers, and all data were acquired using a 10-Hz alternation rate (or 20 Hz in the case of $XerC^{KQ}D$ experiments), with excitation powers of 1 mW for each laser. Fluorescence emission was collected by the objective and separated from the excitation light by a dichroic (545 nm/650 nm; Semrock) and cleanup filters (545 mLP, Chroma; and 633/25 nm notch filter, Semrock). The emission signal was focused on a rectangular slit to crop the image and then spectrally separated, using a dichroic (630-nm DRLP; Omega), into two emission channels, which were focused side by side onto an EMCCD camera (Andor iXon 897). The EMCDD was set to an EM gain of 300, corresponding to an approximate real gain of 4.55 counts per photon.

Sample Preparation. Biotinylated DNA was immobilized to the surface of a PEG-passivated coverslip using biotin–NeutrAvidin interactions and sealed using a silicone gasket (Grace Bio-laboratories) and a second coverslip as a lid. Imaging was performed in a buffer consisting of 50 mM Tris·HCl (pH 7.5), 50 mM NaCl, 5 mM $MgCl_2$, 100 $\mu g \cdot mL^{-1}$ BSA, and 1 mM UV-treated Trolox. An enzymatic oxygen scavenging system consisting of 1 $mg \cdot mL^{-1}$ glucose oxidase, 40 $\mu g \cdot mL^{-1}$ catalase, and 1.4% (wt/vol) glucose was added just before sealing the sample before image acquisition. All experiments were performed at a room temperature of 21 °C.

Data Analysis. Fluorescence intensities were extracted from images using previously described TwoTone software (4). The apparent Förster resonance energy transfer (FRET) was calculated using the area under the Gaussian fit to the donor emission under donor excitation, F_{DD}; and the area under the Gaussian fit to the acceptor emission under donor excitation, F_{DA}; using the following:

$$E^* = \frac{F_{DA}}{F_{DD} + F_{DA}}.$$

The point spread function (PSF) widths in all channels were obtained from the mean widths of the fitted elliptical Gaussians. A combination of manual and hidden Markov model (HMM)-based time trace segmentation were used to construct E^* histograms for each FRET state. Histograms were fit with a Gaussian using nonlinear least-squares fitting in MATLAB.

HMM for Data Extraction. HMM can be used as a means of resolving FRET states present in noisy data (5). In a Markov model, the probability of a transition depends only on the present state of the system. HMM refers to the hidden nature of the underlying state, which can produce a range of outputs at each time point sampled. We used Seneca, a package written by Kristofer Gryte (Oxford) (6, 7). The states extracted by HMM were categorized according to their FRET efficiency and the states that preceded them. According to these categories, data belonging to particular structural states were plotted together in histograms and fit (Table S3). Data immediately before or after a transition were discarded to minimize camera integration time effects (8).

Accurate FRET. To convert from measured emission intensities into a distance we corrected for donor leakage into the acceptor emission channel, l; direct excitation of the acceptor, d; and the combined effect of differing detection efficiencies and quantum yields between the fluorophores, γ (9). The accurate FRET is given by the following:

$$E = \frac{DA_{correct}}{\gamma F_{DD} + DA_{correct}},$$

where the corrected acceptor emission under donor excitation:

$$DA_{correct} = F_{DA} - lF_{DD} - dF_{AA},$$

and

$$\gamma = \frac{\Delta DA_{correct}}{\Delta F_{DD}},$$

where $\Delta DA_{correct}$ is the change in $DA_{correct}$ either side of a change in FRET state, and ΔF_{DD} is the change in F_{DD} either side of the same transition. Transitions, rather than photobleaching events

(10), are chosen because they are much more frequent in our data and hence allow us to confirm that variation in γ between states in our recombination pathway is small, supporting our use of a mean γ for all populations and molecules from a particular substrate.

The Förster radius, R_0, was calculated from the refractive index of the medium, $n = 1.33$; the normalized fluorescence emission spectrum of the donor, $f_D(\lambda)$; the acceptor molar extinction coefficient, $\epsilon_A(\lambda)$; the quantum yield of the donor, Q_D; and the orientation factor, κ^2, according to the following:

$$R_0 = 0.211\left(\kappa^2 n^{-4} Q_D J\right)^{1/6}$$

$$J = \int f_D(\lambda)\epsilon_A(\lambda)\lambda^4 d\lambda.$$

The emission and absorption spectra were measured on a fluorometer (Photon Technology International) for singly labeled central regions of substrates I and II, in the presence of WT XerCD in the same buffer as the recombination experiments, but without Trolox or the oxygen scavenging system. A literature value of 0.67 was assumed for Q_D (11). The orientation factor was assumed to be 2/3. A Perrin plot of the anisotropy was used to estimate the freedom of each fluorophore relative to its attachment point, and this allowed an estimate of the 67% confidence interval for κ^2 using FRETnps software (12). The errors were propagated (13) and the distance calculated (Table S2).

The uncertainty in each of the accurate FRET distances is ~10 Å, the majority of which can be attributed to our uncertainty in the value of the orientation factor for the fluorophores, κ^2. We can compare distances predicted using a Cre–*loxP* structure (Table S1), with our three substrates, and observe broad agreement with the predicted distances. Using multiple independent labeling schemes to investigate structure allows us to mitigate the effect of this orientational uncertainty (14).

The smallest accurate FRET that we could reliably distinguish from the background due to leakage and direct excitation was established using a Rayleigh criterion and a kinetic Monte Carlo Markov chain simulation. The simulation explicitly simulated photon emission times in each channel with the appropriate cross talks, electron multiplying gain by the CCD, read noise, and the least-squares fitting to the PSF. The photon count was chosen to match the width of the $E^* \approx 0.72$ population in substrate II, which accounts for the excess heterogeneity found in the study by Holden et al. (4). It was found that $E^* \approx 0.20$ would just be resolvable against our background, corresponding to a maximum measureable distance of around 90 Å. Hence, any states in the recombination pathway with no apparent FRET correspond to an interfluorophore distance of >90 Å.

Rate Determination. The transition rates, $k = 1/\tau$, quoted in this work (Fig. 5) have been extracted using maximum-likelihood fitting in MATLAB (Figs. 2–4 and Figs. S3 and S4) using the probability density for a dwell, t, of the following:

$$p(t) = ke^{-kt}.$$

A more complicated kinetic scheme was apparent in substrate III, where reverse transitions were observed (Fig. S4*B*):

$$\text{XerC-HJ} \overset{k_-,k_+}{\longleftrightarrow} \text{XerC-Product} \xrightarrow{k_2} \text{Dissociation}$$

The rates k_+ and k_- refer to the forward and backward rates for XerC–HJ converting to XerC–P, and k_2 refers to the dissociation rate of XerC–Product. The summed dwells in XerC–P, $t_{\sum XerC\text{-}P}$ (i.e., the total time the molecule spends in XerC–P before dissociation), for each molecule should follow the probability density:

$$p\left(t_{\sum XerC-P}\right) = k_2 e^{k_2 t_{\sum XerC-P}},$$

and the dwell time spent in XerC–HJ before each transition to XerC–P, $t_{XerC-HJ}$, should follow:

$$p(t_{XerC-HJ}) = k_+ e^{-k_+ t_{XerC-HJ}}.$$

The dwell time spent in XerC–P before either a dissociation or a backward transition to XerC–HJ, t_{XerC-P} should follow:

$$p(t_{XerC-P}) = (k_2 + k_-)e^{-(k_2+k_-)t_{XerC-P}}.$$

These distributions can again be fit to the data using maximum-likelihood estimation in MATLAB, and the rates can all be deduced (Fig. S4*B*).

Reverse transitions for the other steps in the reaction pathway were rarely observed (<4 molecules in each dataset of ~200 molecules). From this, we can calculate an upper bound on the reverse rates (Fig. 5). We note that, for each state in the pathway, given a forward transition rate k_f and a backward rate k_b, the probability of observing less than m reverse transitions in N molecules is given by the following:

$$p(<m) = \sum_{0<i<m} \left(\frac{k_f}{k_b + k_f}\right)^{N-i} \left(\frac{k_b}{k_b + k_f}\right)^{i} \frac{N!}{(N-i)!i!}.$$

We choose our limiting backward rate such that were the "true" backward rate faster than our limit, our data (fewer than m reverse transitions) would have been observed less than 5% of the time. Setting $p = 5\%$; $m = 4$ and $N = 249$, 134, or 111 for substrates I, II, and III; and k_f to the forward rate for the appropriate transition, we can solve the above for k_b (Fig. 5).

1. Pinkney JNM, et al. (2012) Capturing reaction paths and intermediates in Cre-loxP recombination using single-molecule fluorescence. *Proc Natl Acad Sci USA* 109(51): 20871–20876.
2. Ferreira H, Sherratt DJ, Arciszewska LK (2001) Switching catalytic activity in the XerCD site-specific recombination machine. *J Mol Biol* 312(1):45–57.
3. Massey TH, Mercogliano CP, Yates J, Sherratt DJ, Löwe J (2006) Double-stranded DNA translocation: Structure and mechanism of hexameric FtsK. *Mol Cell* 23(4):457–469.
4. Holden SJ, et al. (2010) Defining the limits of single-molecule FRET resolution in TIRF microscopy. *Biophys J* 99(9):3102–3111.
5. Jung S, Dickson RM (2009) Hidden Markov analysis of short single molecule intensity trajectories. *J Phys Chem B* 113(42):13886–13890.
6. Uphoff S, Gryte K, Evans G, Kapanidis AN (2011) Improved temporal resolution and linked hidden Markov modeling for switchable single-molecule FRET. *ChemPhysChem* 12(3):571–579.
7. Le Reste L, Hohlbein J, Gryte K, Kapanidis AN (2012) Characterization of dark quencher chromophores as nonfluorescent acceptors for single-molecule FRET. *Biophys J* 102(11):2658–2668.
8. Bronson JE, Fei J, Hofman JM, Gonzalez RL, Jr., Wiggins CH (2009) Learning rates and states from biophysical time series: A Bayesian approach to model selection and single-molecule FRET data. *Biophys J* 97(12):3196–3205.
9. Lee NK, et al. (2005) Accurate FRET measurements within single diffusing biomolecules using alternating-laser excitation. *Biophys J* 88(4):2939–2953.
10. Ha T, et al. (1999) Single-molecule fluorescence spectroscopy of enzyme conformational dynamics and cleavage mechanism. *Proc Natl Acad Sci USA* 96(3):893–898.
11. Cooper M, et al. (2004) Cy3B: Improving the performance of cyanine dyes. *J Fluoresc* 14(2):145–150.
12. Muschielok A, et al. (2008) A nano-positioning system for macromolecular structural analysis. *Nat Methods* 5(11):965–971.
13. Uphoff S, et al. (2010) Monitoring multiple distances within a single molecule using switchable FRET. *Nat Methods* 7(10):831–836.
14. Rasnik I, Myong S, Cheng W, Lohman TM, Ha T (2004) DNA-binding orientation and domain conformation of the *E. coli* rep helicase monomer bound to a partial duplex junction: Single-molecule studies of fluorescently labeled enzymes. *J Mol Biol* 336(2): 395–408.

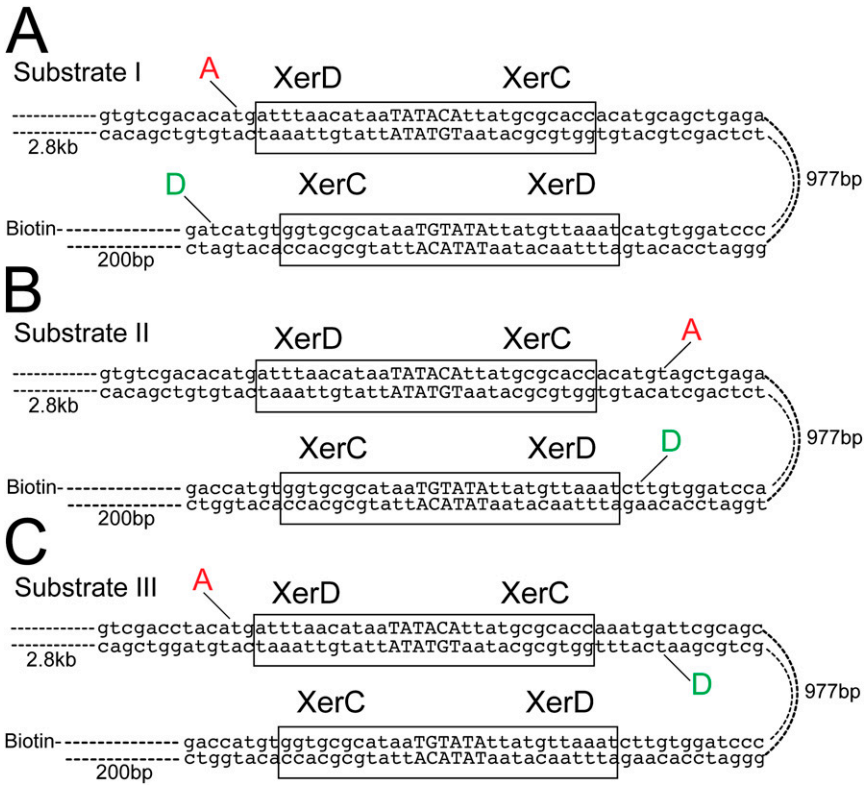

Fig. S1. Sequences and labeling positions of DNA substrates used throughout this study. *dif* sites are boxed and the 1-kbp–long DNA fragment linking two *dif* sites is represented by dashed lines. XerC and XerD binding sites are indicated with the name of the relevant protein. The red A indicates the attachment of Cy5 using a C6-linker, and the green D indicates the attachment of Cy3B using another C6-linker. (*A*) Substrate I. (*B*) Substrate II, designed to show FRET in intermediates preceding HJ isomerization and to investigate the stability of the product. (*C*) Substrate III, which was designed to show FRET in intermediates following HJ isomerization.

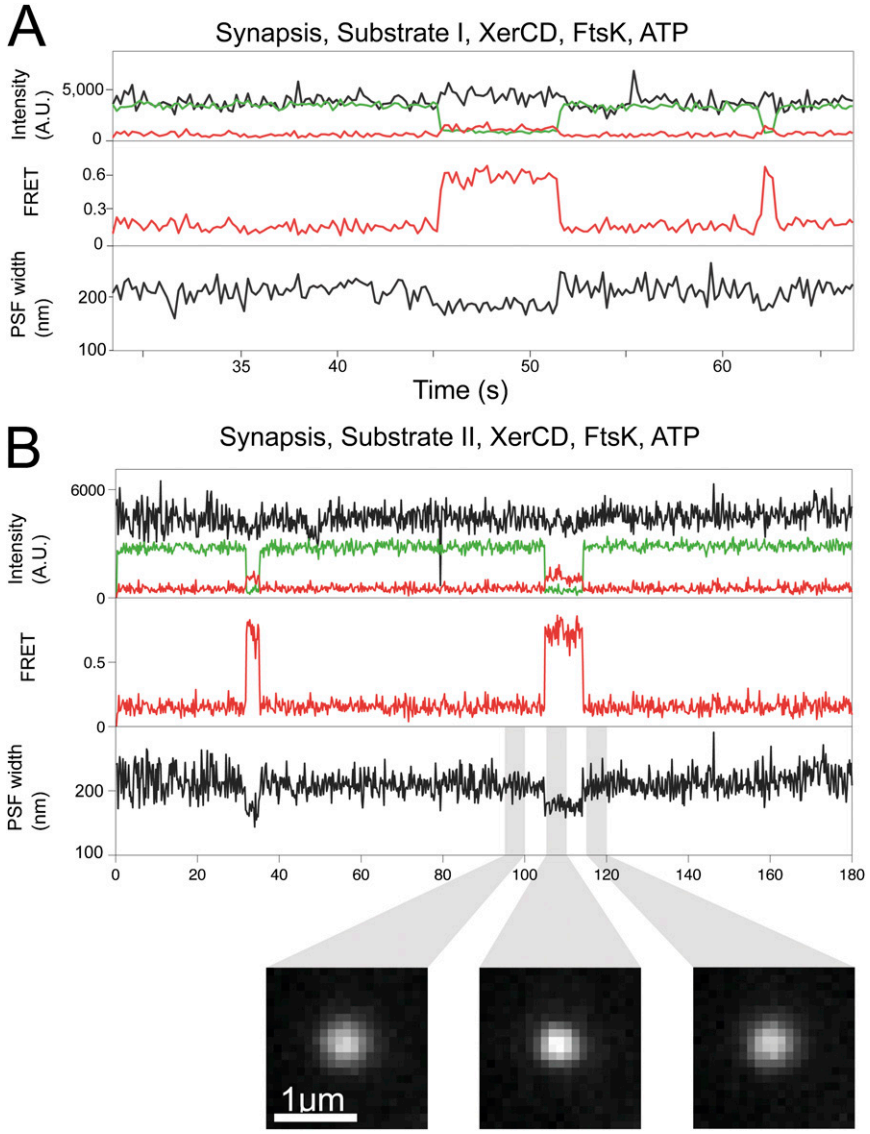

Fig. S2. Synapsis formation within substrates I and II in the presence of FtsK and ATP. (*A*) Time trace showing reversible synapsis formation in substrate I. Loading of FtsK was a limiting factor in recombination on the surface and substrate I would undergo repetitive synapsis formation until activated by FtsK. (*B*) Time trace showing synapsis events in the presence of FtsK in substrate II. PSF examples before, during, and after synapsis were made by averaging 25 frames (highlighted in gray). During synapsis, the PSF is narrower, which acts as our tethered fluorophore motion observable.

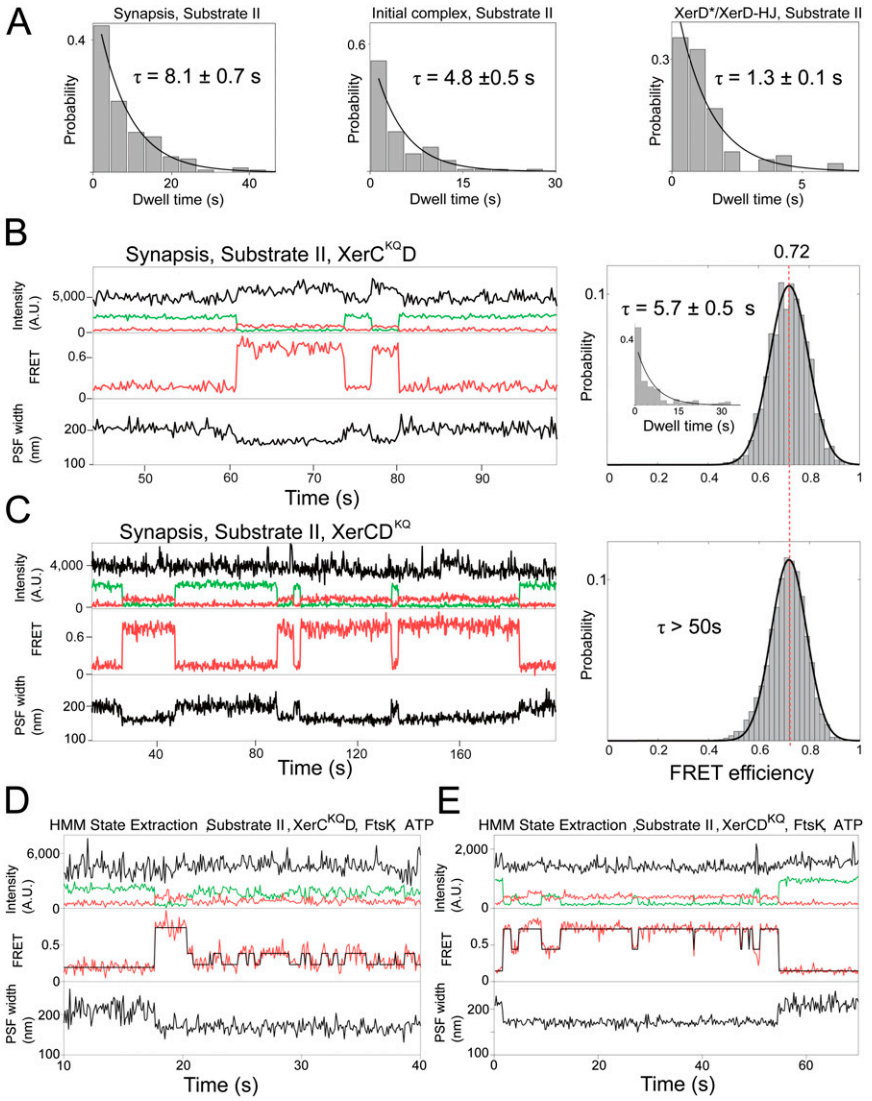

Fig. S3. Substrate II: dwell time analysis, synapsis with XerC^{KQ} and XerD^{KQ} mutants, and HMM for state extraction. (*A*) Dwell time histograms corresponding to lifetimes in Fig. 3 *B* and *C*. The mean lifetime, τ, was obtained from a one parameter exponential fit to the data using MATLAB. (*B* and *C*) In the absence of FtsK–ATP the XerC^{KQ}D and XerCD^{KQ} protein combinations formed complexes similar to the WT XerCD. (*D*) Time trace showing oscillations between XerD–HJ ($E^* \approx 0.37$) and XerC–HJ ($E^* \approx 0.18$), in an experiment using XerD and a catalytic mutant, XerC^{KQ}. The black line in the *Middle* shows the HMM idealized time trace, used to identify transition times for data extraction. (*E*) Time trace showing repeated activation of the synaptic complex formed by XerC and XerD^{KQ}. The black line in the *Middle* shows the HMM idealized time trace, used to identify transition times for data extraction.

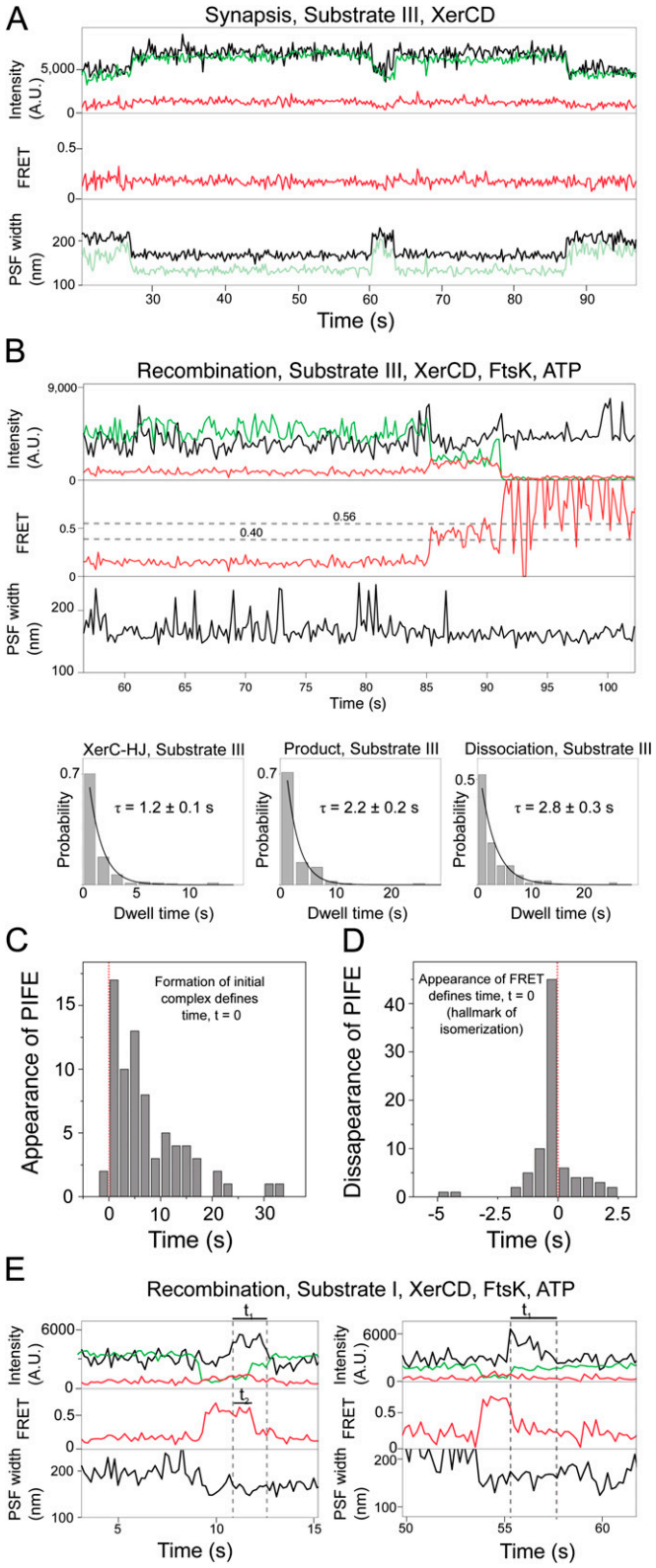

Fig. S4. Substrate III synapsis and dwell time analysis; and protein-induced fluorescence enhancement (PIFE). (*A*) Simultaneous narrowing of donor and acceptor PSFs indicates the formation of synaptic complex in substrate III. Additionally, increases in the intensity of both fluorophores indicate that they are closer to the surface within the evanescent excitation field. Without FtsK and ATP, these complexes reverted back to substrate. (*B*) Example time trace and dwell time histograms for substrate III. The time trace shows transitions between XerC–HJ ($E^* \approx 0.56$) and XerC–P ($E^* \approx 0.40$) before dissociation. All data were fit with single-parameter exponential decays in MATLAB. Occasional interconversions back to XerC–HJ from product DNA were observed. To quantify this rate, the dwells for product transitioning to either dissociation or back to XerC–HJ were fit to recover the total transition rate from product (*Middle*). The dwell time for product to dissociate was also fit (*Right*), and the rate of backward stepping from product to XerC–HJ was determined as the difference between these rates.

Legend continued on following page

(*C*) A histogram of the timing of the appearance of PIFE relative to the timing of formation of the initial synapsis. The distribution indicates that FtsK arrives after the formation of the initial complex, showing that the initial synapsis is the substrate for FtsK activation. (*D*) Disappearances of PIFE relative to HJ isomerization (appearance of FRET). In the majority of events, PIFE ceases just before HJ isomerization. (*E*) PIFE in substrate I. Around 50% of events were accompanied by PIFE in substrate I. Time t_1 corresponds to presence of FtsK near the synaptic complex. Time t_2 is the time needed for the induction of the conformational switch from initial complex to XerD*.

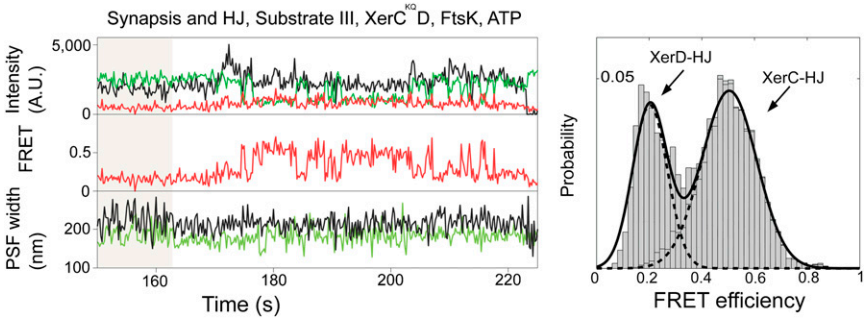

Fig. S5. HJ isomerization in substrate III with XerC^{KQ}, WT XerD, FtsK, and ATP. We see isomerization between a state with $E^* \approx 0.20$ and $E^* \approx 0.50$, and we conclude that $E^* \approx 0.20$ corresponds to XerD–HJ in this substrate. $E^* \approx 0.50$ is lower than the $E^* \approx 0.56$ in the WT complexes, because rapid transitions to XerD–HJ and back within a single frame will skew the distribution toward a lower apparent FRET.

Table S1. Substrate design and predicted interfluorophore distances for possible states in the recombination pathway

	Distance, Å			
Substrate	XerC*–Substrate	XerD*–Substrate	XerC*–Product	XerD*–Product
Substrate I	65	104	107	82
Substrate II	95	85	93	106
Substrate III	107	82	65	104

Distances between fluorophores were inferred from the Cre crystal structure in different nucleoprotein conformations. We performed three radii accessible volume calculations using software described in Sindbert et al. (1) using 2HOI (2). We used the mean fluorophore positions to estimate their separation. The DNA arms were extrapolated and their position relative to the active/inactive cleavage site was calculated by identifying which strand would be next cleaved in any structure and counting the appropriate number of base pairs on the correct strand in the right direction.

1. Sindbert S, et al. (2011) Accurate distance determination of nucleic acids via Förster resonance energy transfer: Implications of dye linker length and rigidity. *J Am Chem Soc* 133(8):2463–2480.
2. Ghosh K, Guo F, Van Duyne GD (2007) Synapsis of loxP sites by Cre recombinase. *J Biol Chem* 282(33):24004–24016.

Table S2. Accurate FRET efficiencies and distances calculated for all identifiable states in all substrates

Population	Accurate FRET	SD	Distance, Å	Uncertainty in distance, Å
Substrate I				
Synapsis	0.68	0.02	58.6	8.8
Recombination	0.70	0.02	57.6	8.7
Substrate II (XerCD)				
Synapsis	0.84	0.01	51.6	7.7
Initial complex	0.82	0.02	53.2	8.0
XerD–HJ	0.39	0.06	73.5	11.4
XerC–HJ/XerC–P	<0.2		>90	
Substrate II ($XerC^{KQ}D$)				
Initial start	0.83	0.01	52.4	7.8
Initial end	0.83	0.01	52.6	7.9
XerD–HJ	0.42	0.05	72.0	10.9
XerC–HJ	<0.2		>90	
Substrate II ($XerCD^{KQ}$)				
Initial complex	0.83	0.01	52.4	7.8
XerD*	0.53	0.03	66.8	10.1
Substrate III				
XerC–HJ	0.72	0.01	56.7	8.6
XerC–P	0.54	0.02	64.7	9.8

Table S3. Parameters for the Gaussian fits to population histograms of E* FRET efficiencies (Figs. 2–4)

Population	Mean	SEM	SD	SEM of SD
Substrate I				
Synapsis	0.549	0.001	0.082	0.001
Recombination	0.571	0.002	0.111	0.002
Substrate II (XerCD)				
Synapsis	0.720	0.002	0.086	0.002
Initial complex	0.717	0.002	0.101	0.002
XerD*	0.372	0.003	0.106	0.003
XerC–HJ/XerC–P	0.174	0.001	0.050	0.001
Substrate II ($XerC^{KQ}D$)				
Initial start	0.727	0.002	0.095	0.002
Initial end	0.718	0.002	0.097	0.002
XerD–HJ	0.366	0.002	0.079	0.002
XerC–HJ	0.217	0.001	0.061	0.001
Substrate II ($XerCD^{KQ}$)				
Initial complex	0.718	0.001	0.081	0.001
XerD*	0.438	0.004	0.094	0.004
Substrate III				
XerC–HJ	0.559	0.003	0.096	0.003
XerC–P	0.400	0.002	0.078	0.002

The data were extracted manually and using HMM and plotted in a histogram, and then fit with a Gaussian using a nonlinear least-squares method in MATLAB. Then mean and SD are from the fitted curve. The SE in the mean (SEM) is defined as the 1σ-confidence interval on the parameter fit.